Oxygen Evolution and Reduction on Two-Dimensional Transition Metal Dichalcogenides

Naiwrit Karmodak,* Luca Bursi, and Oliviero Andreussi*

Department of Physics, University of North Texas, Denton, TX 76203, USA

E-mail: naiwrit.karmodak@unt.edu; oliviero.andreussi@unt.edu

Abstract

Motivated by the need to find good electrocatalysts for water oxidation and O_2 reduction, composed of non-toxic and earth-abundant elements, a systematic screening of two-dimensional (2D) transition metal dichalcogenides (TMDCs) is performed. To identify compounds that are intrinsically active and can fully take advantage of the high surface area of 2D catalysts, this study focuses on the properties of the ideal basal planes of 2D TMDCs, in the 2H, 1T, and 1T' phases. Roughly two hundred materials proposed in computational databases are studied by means of first-principles-based simulations coupled with continuum embedding models to account for the presence of electrochemical environments. The best candidates with overpotentials for the oxygen evolution and reduction reactions lower than 0.5 V under acidic conditions and higher stability against degradation in electrochemical environments are selected. For OER, the designed workflow identifies one material that is active and thermodynamically stable, with seven more that are metastable at the oxidative potentials and acidic pH. On the other hand, for ORR we obtain 20 materials with overpotentials less than 0.5 V. Among these compounds, the six bifunctional compounds have been experimentally

reported, with 1T-$NbTe_2$ and 1T'-$MoTe_2$ being the best performing catalysts for oxygen evolution and reduction respectively.

TOC Graphic

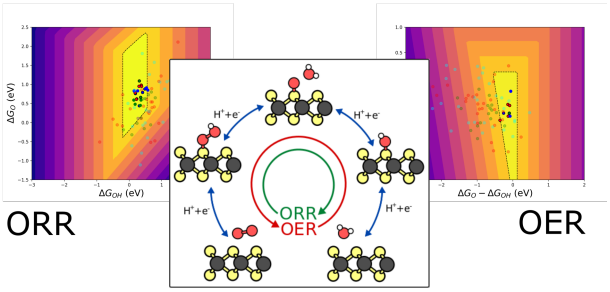

The electrochemical water cycle has gained significant attention in recent years as a sustainable approach for mitigating the global energy demand.[1] Improving the technology for electrochemical splitting of water in an electrolyzer, i.e. acquiring control over the oxygen and hydrogen evolution reactions (OER and HER, respectively), could unlock the potential of intermittent energy resources to generate clean and renewable chemical fuels, like H_2. The reverse reactions are involved in fuel cells, where renewable electrical power is generated by the oxidation and reduction of H_2 and O_2, respectively, to H_2O. The major issue that reduces reaction efficiency in both processes is the high overpotentials associated with the anodic O_2 evolution reaction in electrolysis cells and the cathodic O_2 reduction reaction (ORR) in fuel cells.[2,3] Several efforts have been devoted to identify effective electroctatlysts for both OER and ORR. To date the transition metal oxides IrO_2 and RuO_2 in acidic conditions, and Ni and Fe based oxides in basic conditions are known to be the best electrocatalysts for OER. On the other hand, Pt surface known to be the only suitable electrode material with the lowest overpotential in acidic conditions for ORR.[4,5] However, most of these electrocatalysts are prohibitively expensive and are thus unsuitable for large-scale applications. Therefore, greater number of electrode materials composed of earth-abundant elements with high activity and selectivity are urgently needed.

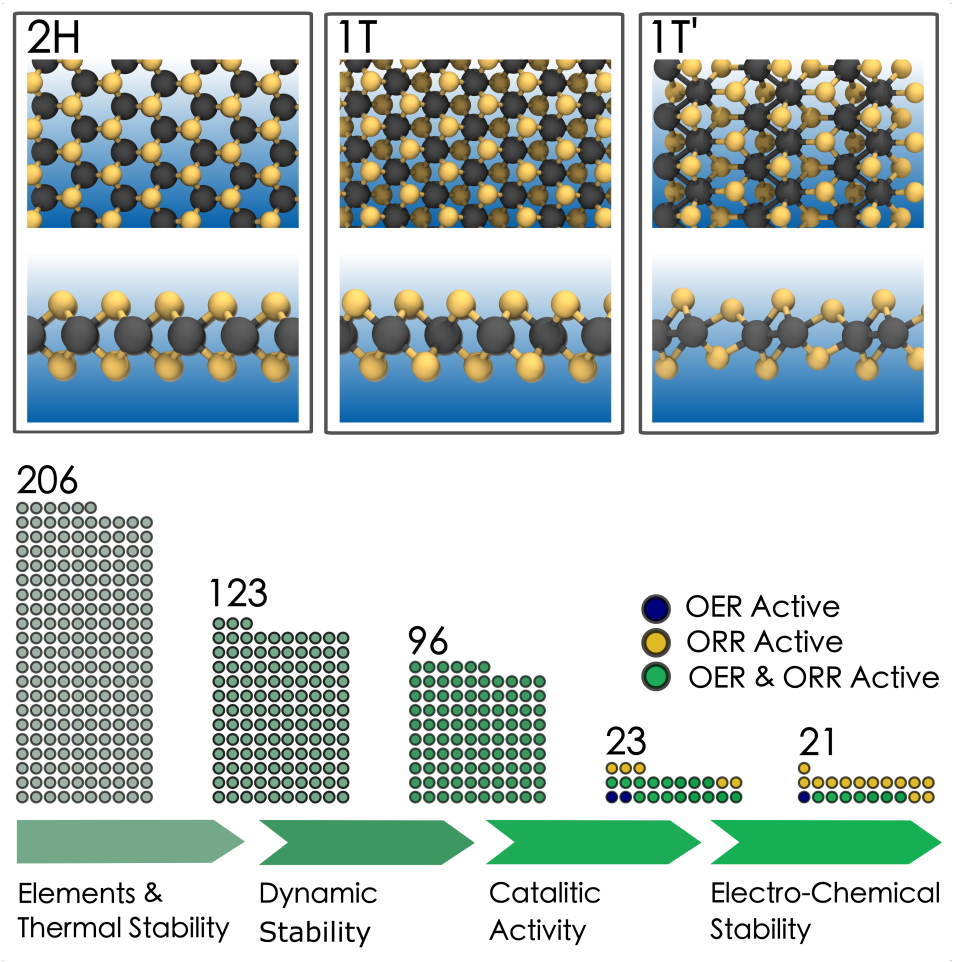

Figure 1: Top panels: Top and side views of the 2H, 1T, and 1T' phases of transition metal dichalcogenides materials, where transition metals and chalcogenide atoms (S, Se, or Te) are visualized as large grey and small yellow spheres, respectively. Bottom panel: Schematic representation of the main steps of the screening workflow. The materials considered at each step are presented by small circles, with the total number reported above. Following the characterization of catalytic activity, materials are distinguished according to whether they are active for oxygen evolution, reduction, or both.

Influenced by the intriguing properties of two dimensional (2D) materials and their successes in various applications,[6–8] efforts are being spent on identifying effective 2D electrocatalysts. Of the large number of known 2D materials, transition metal dichalcogenide (TMDC) monolayers have attracted immense attention, for their accessible synthesis,[9] higher thermodynamic and mechanical stability,[10,11] and interesting electronic properties.[12,13] 2D TMDCs have a chemical formula of MX_2 and are composed of three atomic layers, with one transition-metal (M) layer sandwiched between the two chalcogenide (X = S, Se, and Te) layers. Three alternative atomic arrangements of the chalcogenide layers have been observed for 2D TMDC systems, denoted as 2H, 1T, and 1T' in the top panels of Figure 1.[9,14] While in the 2H structure the two chalcogenide layers are stacked in an AA arrangement, in both the 1T and 1T' phases, the chalcogenide layers form an AB stacking, with one layer slightly displaced with respect to the other. The different atomic arrangements give rise to significant differences in structural and catalytic properties, resulting in a large variety of applications.[12,15] In recent years, several 2D TMDC systems have been explored as potential catalysts for the hydrogen evolution reaction (HER),[8,16–18] while their electrocatalytic activity for both ORR and OER has been less characterized.[15,19–22] Nonetheless, depending on the composition (the transition metals and surface chalcogen atoms), and structural morphology, 2D TMDCs could show favorable electrocatalytic activity for both OER and ORR.

We recently combined a continuum model of the embedding electrolyte-solution environment with a rigorous first-principles thermodynamic approach for electrochemical simulations to develop an effective computational workflow for screening 2D electrocatalysts for HER, based upon the reaction efficiency and electrochemical stability.[23] In the present study we use a similar approach, visualized in the bottom panel of Figure 1, to explore the electrocatalytic applications of different TMDC monolayers composed of earth-abundant elements for OER and ORR. To characterize the reaction efficiency we calculate grand-potential interface energies for the 2D materials covered with the identified intermediate adsorbates. By prop-

erly accounting for the effect of the electrochemical environment on the pristine interfaces we identify several 2D TMDCs with high electrocatalytic efficiency.

Similar to previous approaches in the literature, the present screening process relies on steps of increasing computational complexity. The first two steps are based on simulations performed in vacuum. In the third and fourth steps, simulations are performed in the presence of an aqueous medium, where environmental effects due to solvent molecules and electrolyte ions are accounted for via a continuum solvation scheme defined by the Self-Consistent Continuum Solvation (SCCS) water model.[24] To incorporate the effects of electrolyte ions, we model the electrochemical diffuse layer using Gaussian-shaped counter-charge layers of 0.25 Å thickness, placed symmetrically on both sides of the 2D surface at a distance of 5 Å from the outermost atomic layers.[25,26] The thermodynamic binding energies are determined at a solvent pH of 1 and at different applied potentials using the grand-canonical potential simulation scheme.[27] Further computational details are reported in the supplementary information (SI).

The initial TMDC monolayers are taken from the C2DB[10] and Materials Cloud[11] computational databases of 2D materials. The TMDC compounds from the two databases are first screened according to their thermodynamic stability as determined by first-principles calculations in vacuum in both these databases. In addition, compounds containing Pt, Pd, and Hg atoms are removed, in order to consider only materials composed of earth-abundant and non-toxic elements. In particular, 33 compounds are extracted from the Materials Cloud database, corresponding to easily exfoliable TMDC, with computed vacuum exfoliation energies less than 35 meV/Å^2. From the C2DB structures, we selected the TMDC monolayers with a heat of formation less than E_{hull} + 0.2 eV/atom, where E_{hull} is the convex hull energy of the most stable bulk phase of similar chemical composition. Combining the materials from both databases and removing common candidates we finally obtain 123 compounds.

In the second screening step, the dynamic stability of the materials is determined from their computed phonon frequencies as reported in the corresponding databases. Strictly

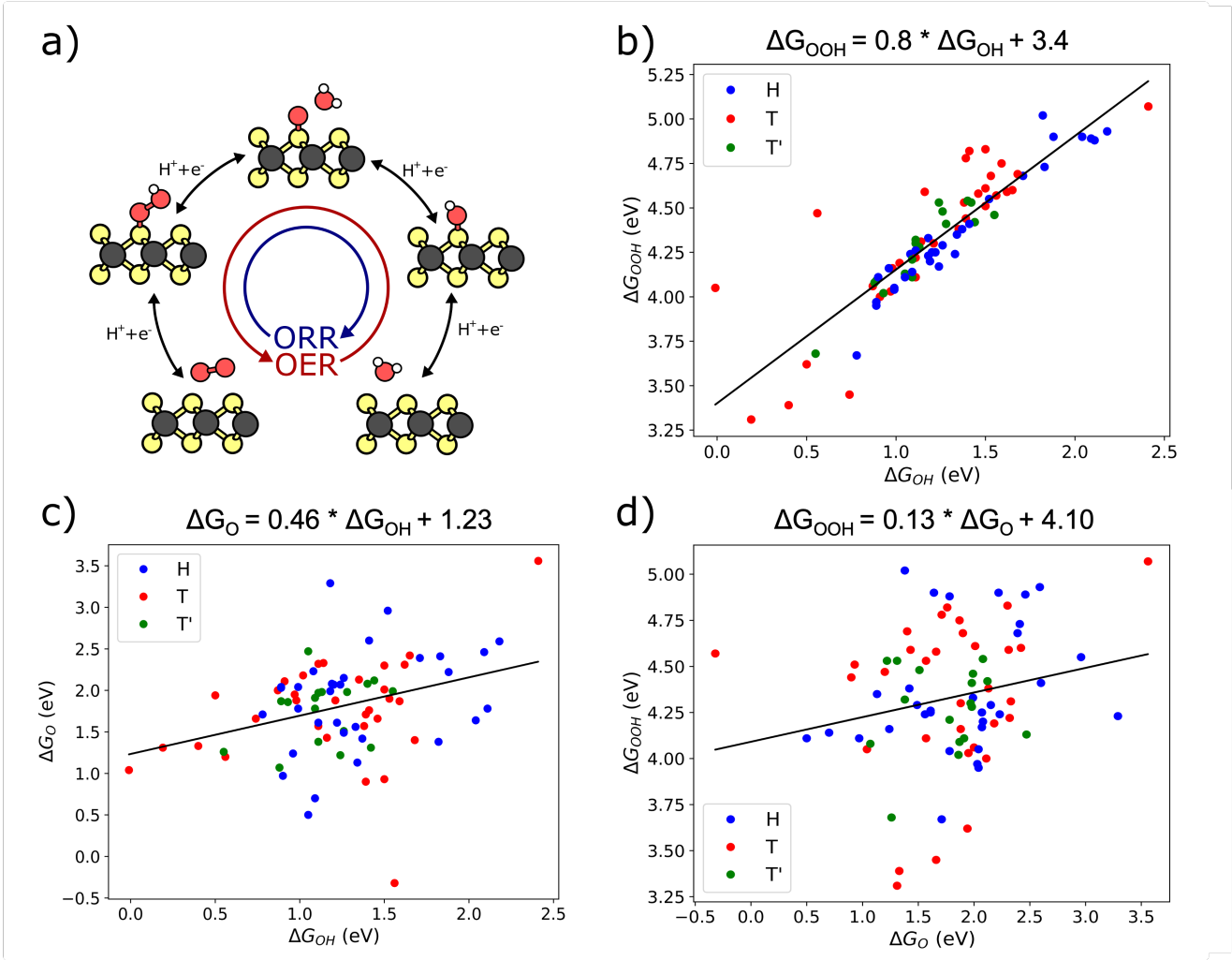

Figure 2: a) Schematic representation of the single-site catalytic steps considered in this study for oxygen evolution and reduction reactions. Oxygen and hydrogen atoms are visualized in red and white, respectively. transition metal and chalcogen (S, Se, or Te) atoms visualized in grey and yellow, respectively. For clarity, only the 2H structure is shown. b-d) Relationships between formation free energies of the three catalytic intermediates: OH^*, O^*, and OOH^*. While a clear linear correlation between the energies of OH^* and OOH^* is observed for all the materials and phases considered (panel b), the formation of O^* does not show a clear trend with the energies of the other catalytic steps (panels c-d).

positive hessian eigenvalues are usually required to identify a kinetically stable material. However, some 2D materials, such as 1T-MoS_2, 1T-VTe_2 and 1T-TiS_2, have been successfully synthesized despite having theoretical hessian eigenvalues as low as -2 eV/Å^2 .[28–30] This suggests that a more relaxed screening criterion may be required. Hence, for the purpose of our screening materials with minimum hessian eigenvalues greater than -2 eV/Å^2 are considered stable. Of the 123 thermodynamically stable candidates, 96 materials are selected, comprising of 35 monolayers with the 2H phase, 39 with the 1T phase, and 22 with the 1T' phase. Among these compounds, 30 monolayers having been identified as easily exfoliable and could be obtained by the exfoliation of their corresponding 3D van-der-Waals bulk solids. The rest of the materials could be synthesized on metal templates using vapor deposition techniques.

While the first selection criteria only depends on intrinsic properties of the compounds, studying the activity and stability of the monolayers requires the characterization of their interaction with catalytic species. For both OER and ORR, a four-step proton-coupled electron transfer (PCET) mechanism involving the three reaction intermediates OH^*, O^*, and OOH^* is reported to be the most favorable one among the predicted reaction pathways.[2,31] Therefore, in this study, we consider the reaction mechanisms shown schematically in the top panel of Figure 2.

First, the adsorption free energies of all reaction intermediates on all possible surface sites are computed in vacuum. The most favorable adsorption sites are determined by relaxing the surface structure of a 2x2 supercell of the 2D material with a single adsorbate placed on main catalytic sites (hollow, on-top, and bridge positions). The adsorption free energy values are calculated using the computational hydrogen electrode (CHE) method,[31] which relies on knowledge of the standard electrochemical reaction potentials.

For all intermediate species, hollow sites, where the intermediates are placed above the three-atom center of the surface chalcogen groups, are the least preferred. In all of the materials, the OH and OOH species have identical preferences for adsorption sites. In particular,

the most preferable adsorption site is found to be on-top. Depending on the elemental composition, some compounds favor a distorted configuration with the adsorbates slightly shifted toward the bridge sites. However, the adsorption sites for oxygen atoms appear to be less exclusive and to strongly depend on the nature of the compound. The energy of the adsorbed oxygen appears to only weakly depend on whether it is placed on top of a chalcogen atom, on a bridge site, or in an intermediate, distorted configuration.

Screening for the preferred binding sites also allows us to determine the structural stability of the materials in the presence of surface adsorbates. In fact, upon adsorption of these intermediate catalytic species, all of the materials but one are found to be stable. However, a significant structural reorganization is observed for 2H-$MoSe_2$ in the presence of OH adsorbates. Due to its reduced stability, this compound has not been included in the following characterizations.

Starting from the most preferable binding sites, electrosorption free energy ($G^{sol}_{ads}(\Phi)$) values for the intermediates in the presence of an aqueous medium are determined using the grand-canonical scheme and the following formula

$$\Delta G^{sol}_{ads}(\Phi) = J_{XH^*}(\Phi) - J_*(\Phi) + \Delta E_{ZPE} - T\Delta S_{ads} \tag{1}$$

where $J_{XH^*}(\Phi)$ and $J_*(\Phi)$ are the grand-canonical free energies of the 2D material surface with and without the adsorbed intermediates, respectively, and ΔE_{ZPE} and $T\Delta S_{ads}$ are the zero-point energy and entropic corrections. Section I in the SI provides further details and the calculation for determining these values. Calculations are performed with a 25% surface coverage of adsorbed species, to avoid non-trivial inter-adsorbate interactions at higher concentrations. The formation of complex adsorption networks would reduce the interaction of the absorbates with the 2D material surfaces and increase the oxidation potentials. Among the 95 materials obtained from the previous screening steps, ground state electronic structure calculations for 13 compounds fail to converge in the presence of large positive surface charges.

The calculated grand-canonical free energies of the three relevant intermediates represent the key quantities to identify catalytically active materials. Following a strategy inspired by the computational hydrogen electrode approach, the interface free energies computed at zero applied potential and neglecting the effects of pH allow us to distinguish potential-determining steps and verify the presence of scaling relations. Correlations between free energies of different interfaces reduce the flexibility in the search for optimal catalysts. While these constraints may significantly limit the performance of the considered materials, they also reduce the dimensionality of the problem and provide clear thermodynamic descriptors for the catalytic activity.

For TMDC monolayers, the binding affinity of the O^* interface with respect to both OH^* and OOH^* intermediates shows no clear correlations, as shown in Figure 2 (c) and (d). However, a linear relationship is observed between OH^* and OOH^* intermediates. By fitting the computed values, we obtain a slope nearly equivalent to unity and an intercept of 3.40 eV. These values are in close agreement with transition metals and their oxides.[2,3] Compared to both 2H and 1T' TMDC monolayers, materials with the 1T structure show more marked deviations from linearity, as shown in Figure 2 (b). The largest deviations are observed for 1T-MoS_2, 1T-VSe_2 and 1T-$ScSe_2$.

Due to this scaling relationship, the difference between the electrosorption energy for OH and OOH species is constant and independent of the nature of the material. The potential-limiting step defining the overall reaction efficiency of the catalysts is thus strongly controlled by the binding affinity of the O atom. We stress here that these findings are consistent with structural information obtained from the simulations, in particular, with the observed similarity in preferred absorption site for OH and OOH. In contrast, the observed change in preferred O adsorption site for many compounds is associated with the absence of clear scaling relationships.

The links between intermediate free energies have strong implications on the catalytic steps limiting the activity of the material. The large intercept of the scaling relationship,

i.e. the large free energy difference between OH^* and OOH^* formation, implies that at least one of the catalytic steps connecting the two intermediates is significantly larger than that of the reference potential of 2.46 V known for an ideal catalyst.[2] The standard CHE approach would exploit this information by only focusing on the potential-limiting steps. This would correspond to the two intermediate steps for OER, and to the first and last step for ORR. More refined approaches that rely on information from all catalytic steps have been proposed in the literature to reduce potential limitations, possibly including kinetic effects and the effect of an applied overpotential.[32,33,34] Furthermore, the recently introduced grand-canonical scheme is shown to effectively account for surface relaxation in charged environments and to provide a more robust evaluation of the catalytic overpotential.[23,35] For this reason, the grand-canonical scheme has been selected as the method of choice in our screening workflow. Differences in performance of alternative approaches are reported in the Supporting Information.

In the third step of the screening workflow, materials with catalytic overpotentials for OER or ORR lower than 0.5 V are selected. In a recent study, the quantitative analysis of the reaction overpotentials for real catalysts have shown that the reference potentials could largely vary within the potential range of 2.16 V to 2.76 V.[34] However, we have calculated the overpotential values with respect to the reference potential of an ideal catalyst as defined by Man et. al. and the other recent computational screening studies for OER and ORR electrocatalysts.[2,44,45] Overall, we identify 16 compounds that could be active for both OER and ORR, plus 2 and 5 additional compounds that exhibit low overpotentials only for OER or ORR, respectively. The chemical formula and corresponding reaction overpotentials for these materials are shown in Table 1.

While a low overpotential is a necessary condition, stability in electrochemical environments, in particular, in the presence of applied potentials, represents an additional stringent requirement for a good electrocatalyst. Therefore, in the last screening step of our computational workflow, the thermodynamic and kinetic barriers for material degradation are

Table 1: TMDCs identified as potential electrocatalysts for OER and ORR, obtained after the first three computational screening steps shown in Figure 1(b). η^{OER} and η^{ORR} are the corresponding overpotentials in V. In column 4 and 5, ΔG_{Th} and ΔE_{kin} denote the thermodynamic free energies and kinetic barrier, respectively, for the formation of decomposition products from the adsorbed O^* intermediate. The decomp. pdts are most stable decomposition products. The corresponding stability pattern is based on ΔG_{Th} and ΔE_{kin} values. Further details are given in main text. References for sythesized TMDCs are given in the last column.

materials	η^{OER}	η^{ORR}	ΔG_{Th}	ΔE_{kin}	decomp. pdts	stability	Exp. Ref.
				2H			
NbS_2	0.46	0.41	-0.10	0.28	SO	unstable	Ref.[36]
$NbSe_2$	0.34	0.34	-1.27	1.02	SeO_2	kinetic	Ref.[37]
$NbTe_2$	0.45	0.44	-1.98	0.75	TeO	unstable	-
TaS_2	-	0.46	-0.97	2.43	SO_2	kinetic	Ref.[38]
$TaSe_2$	0.33	0.41	-2.08	0.35	SeO	unstable	Ref.[39]
$TaTe_2$	0.44	0.43	1.07	2.14	TeO	thermodynamic	-
$CoTe_2$	0.34	0.37	-1.59	0.54	TeO	unstable	-
$CrTe_2$	0.33	-	-2.20	1.13	TeO	kinetic	-
VTe_2	0.24	0.33	-0.03	1.11	TeO	kinetic	-
$NiTe_2$	0.40	0.47	0.10	0.71	TeO	thermodynamic	-
				1T			
$NbTe_2$	0.26	0.40	-0.86	2.83	TeO	kinetic	Ref.[29]
$TaTe_2$	0.27	0.30	-1.04	0.95	TeO	kinetic[a]	Ref.[29]
VTe_2	0.29	0.40	-0.35	0.97	TeO	kinetic[a]	Ref.[29]
$NiSe_2$	0.5	0.48	-0.39	0.92	SeO	kinetic[a]	Ref.[40]
$NiTe_2$	0.50	0.36	0.58	0.98	TeO_2	thermodynamic[a]	Ref.[41]
$CoTe_2$	0.42	0.38	0.11	0.89	TeO_2	thermodynamic[a]	Ref.[42]
$CrTe_2$	0.44	-	-0.61	0.66	TeO	unstable	-
				1T'			
$MoTe_2$	0.29	0.29	-1.76	1.01	TeO	kinetic	Ref.[43]
$CoTe_2$	0.39	0.45	-0.67	0.57	TeO	unstable	-
WTe_2	-	0.49	-0.37	0.66	TeO	unstable	Ref.[39]
$RuTe_2$	-	0.41	0.57	1.11	TeO	thermodynamic	-
$OsTe_2$	-	0.33	-0.26	0.68	TeO	unstable	-
$CrSe_2$	-	0.47	-2.03	0.65	SeO	unstable	-

evaluated. In particular, surface oxidation of the monolayers at ambient conditions for OER would lead to oxidative etching of surface chalcogen atoms into various aqueous products. Edge sites are expected to have higher reactivity, due to the lower coordination of surface atoms and a greater accessibility to solvent molecules.[46,47] However, for high surface coverage of O^* intermediates, basal surfaces may also show oxidative decomposition. To explore the probability of these degradation pathways, we characterize the stable configurations and preferable binding sites of O^* up to a 50% basal-surface coverage of the catalytically active compounds.

Most of the screened 2D materials prefer adsorption of multiple O^* intermediates on a single surface site to adsorption on different sites. With this structural arrangement of O^* intermediates, the most probable decomposition pathway that has been observed[48–50] points towards the desorption of the chalcogen atom with either one or both of the attached O atoms, i.e. as XO_2 or XO species, respectively (panel a) of Figure 3). Desorption of these oxidative products will create a surface vacancy. However, the detachment of an XO ion is followed by another reaction step in which the remaining O^* diffuses into the vacancy site. As a result, along with the formation of the aqueous product, in this latter case surface oxidation would also lead to O doping of the material. The section S-V in the SI shows the chemical pathway for the decomposition mechanism.

The initial step leading to the adsorption of O^* intermediates on the basal plane would depend on the applied potential, whereas the desorption of aqueous products, either XO_2 or XO, would be thermally controlled. In particular, the presence of an applied potential would lower the thermodynamic barrier for the formation of O^* intermediates on the basal surface. In this situation, the thermal desorption of XO_2 or XO ion will form the reaction-limiting step, determining the overall propensity towards decomposition. To fully characterize these processes, we calculate both the thermodynamic free energies and kinetic barrier of the desorption pathways. Based on these calculations, materials that are thermodynamically more stable than the decomposition products at oxidative limiting potentials are identified

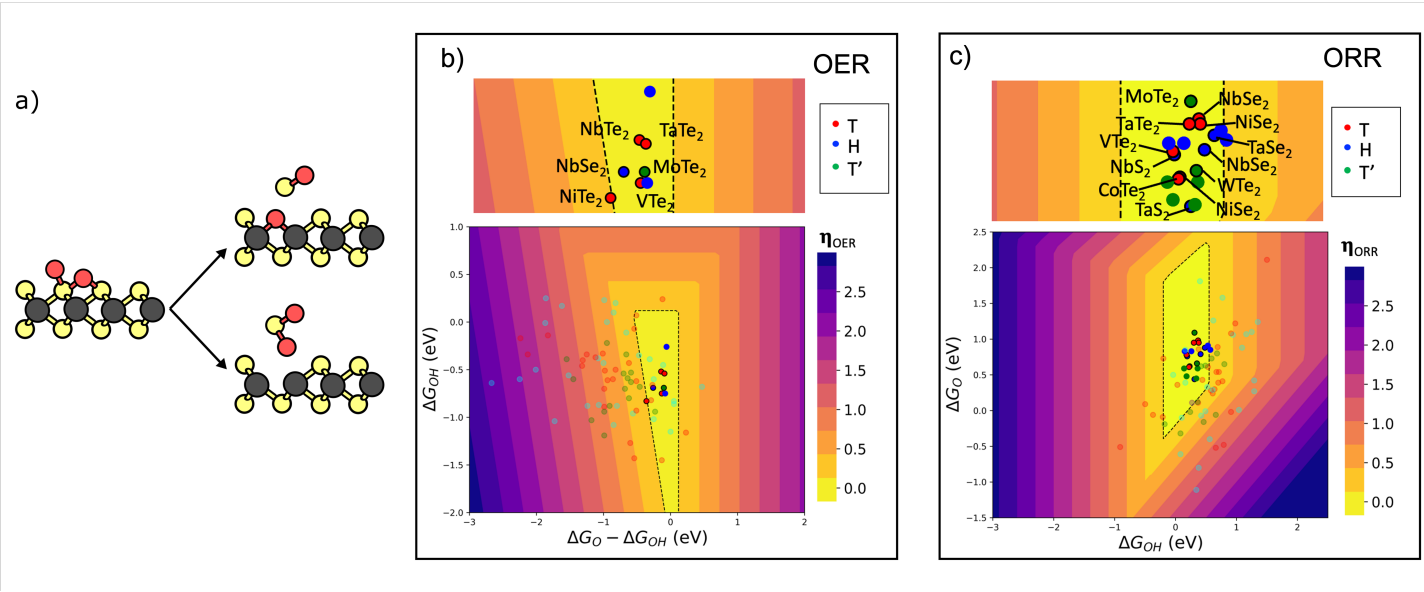

Figure 3: a) Schematic representation of the two decomposition pathways observed for the considered materials in the presence of surface oxides. b-c) Catalytic activity of the materials, as described by the overall reaction free energy at an applied overpotential of 0.5 V, computed using a CHE-approach as a function of intermediates formation free energies. Materials passing the first two screening steps are reported as faded or solid dots, with blue/red/green colors corresponding to 2H/1T/1T' phases, respectively. Solid colored circles identify materials that are found to be stable or metastable under oxidative overpotential values and acidic pH. Black outlines identify materials that have been reported experimentally. Materials in the yellow areas are considered to be catalytically active for OER (b) and ORR (c). Chemical formulas of the stable and active compounds with known synthetic pathways are shown in the top panels.

as promising catalysts. In addition, to account for the possibility of metastable materials, in which the decomposition process is significantly unlikely at standard conditions, compounds with a large kinetic barrier for decomposition are also selected as potential catalysts. A value significantly larger than k_BT at room temperature assures that the deterioration of the material is sufficiently slow. Hence, a specific threshold of 0.9 eV was selected based on the distribution of computed kinetic barriers for the considered materials (as reported in Figure S1 of SI). For materials with multiple intermediate and transient states in the desorption mechanism, the kinetic barrier for the first degradation step is considered as the limiting step to determining kinetic stability.

The desorption free energy, kinetic barrier, and most probable desorbed products for the 23 catalytically active compounds are also reported in Table 1. Overall, 5 compounds are determined to be thermodynamically stable . In addition, 9 compounds for which desorption of oxidation products is computed to be exothermic are observed to have a sufficiently high kinetic stability. Among the 14 selected compounds, 9 have been reported experimentally. The decomposition pathways for these materials are visualized and detailed in the Supporting Information (section S-VI), including some of the experimentally accessible candidates.

Considering the stability criterion against oxidation degradation, we have identified 12 TMDCs as active catalysts for OER. However, the oxidative degradation mechanism shown here for higher O^* coverage will not effect the stability of the materials identified as active catalysts for ORR. Therefore, all the 21 TMDCs screened in the previous step as given in Table 1 are expected as stable electrocatalysts for ORR.

The screening workflow relies on calculations performed with a 25% surface coverage of the intermediates. However, a low surface coverage may not incorporate the effect of inter-adsorbate interactions on the adsorption energetic. Therefore, to determine the extent of inter-adsorbate interactions on the limiting potentials at higher surface coverage, we have calculated the binding energies of OH^*, O^* and OOH^* intermediates with different surface coverage for the most active materials in Table 1. Following the CHE approach, these

energies give access to simplified Pourbaix diagrams (ΔG_{pbx} vs U in RHE scale), which are reported in Figure S7 to S9 in the SI (section S-VII).

We found that, at lower oxidation potentials, ΔG_{pbx} values for the oxygenated intermediates show large variation with surface coverage. However, in the range of potentials at which the selected compounds become ORR active, the most stable phase corresponds to the bare surface of the materials except for 2H-$TaTe_2$, justifying the neglect of inter-adsorbate interactions. For 2H-$TaTe_2$ the 50% O^* covered surface is found to be the most stable surface state. The surface Pourbaix diagrams allowed us to identify 20 TMDC monolayers with higher activity and stability for ORR.

Instead, in the range of potentials required for OER activation on the selected compounds, oxygenated structures become more stable for all OER active materials. Nonetheless, for 8 of the considered stable materials against oxidative degradation (step 4 of screening workflow), the computed inter-adsorbate interactions appear to have small effect on the binding energies of the intermediates. However, 4 materials, 2H-$TaTe_2$, 2H-$NiTe_2$, 1T-$CoTe_2$ and 1T-$NiSe_2$, show an increased stability of O^* adsorbates at higher coverages, suggesting that single adsorbate simulations may substantially underestimate the overpotential for OER. This limitation is particularly severe for 2 compounds, 2H-$TaTe_2$ and 1T-$CoTe_2$, for which a material reconstruction is observed at high O^* coverage. For this reason, these 4 compounds are removed from the final selection of OER active compounds.

Among the compounds selected with higher activity, we have identified seven materials 2H-$NbTe_2$, 2H-VTe_2, 1T-$NbTe_2$, 1T-$TaTe_2$, 1T-VTe_2, 1T-$NiTe_2$ and 1T'-$MoTe_2$ as bifunctional catalysts, active for both OER and ORR. Focusing on materials that have already been experimentally reported, we identify the best performing catalyst for OER or ORR as 1T-$NbTe_2$ and T'-$MoTe_2$, respectively.

In conclusion, we have systematically studied potential 2D-TMDC compounds based on earth-abundant and non-toxic elements as electrocatalysts for oxygen evolution and reduction reactions. The workflow relied on state-of-the-art, first-principles-based simulations

that account for the effects of embedding electrochemical environments. The materials are screened using a four-step process that involved the characterization of material stability and catalytic activity. Starting from more than two hundred 2D compounds catalogued in computational databases, we have identified 23 monolayers with preferable catalytic activity in acidic environments. The reaction overpotential for either ORR or OER are computed to be lower than 0.5 V, thus comparable to the best performing catalysts. Further analyzing the electrochemical stability and surface Pourbaix diagrams, 8 compounds are eventually selected for OER. On the other hand, for ORR we have screened 20 preferable electrocatalysts with lower overpotential values. For several of these monolayers, suitable synthetic pathways have already been reported. Among these compounds, 1T-$NbTe_2$ and T'-$MoTe_2$ are identified as the best performing catalysts for OER and ORR respectively, for which synthetic pathways have been known. We are convinced that the reported trends should motivate further experimental studies and characterizations of catalytic properties of these materials.

Supporting Information Available

The Supporting Information (SI) is available free of charge on the ACS Publications website at DOI: XXXX

The computational simulation methodologies for the free energy calculations with the implicit solvent model has been described in section S-I. section S-II shows the selection criterion for thermodynamic and dynamic stability of the compounds. Section S-III shows the selection criterion for the kinetic energy barrier. A comparison between the grand-canonical and CHE overpotential values is given in section S-IV. section S-V and S-VI show the decomposition pathway and the kinetic energy barriers respectively for oxidative etching under OER potentials. Section S-VII shows the surface Pourbaix plots for the active compounds screened for OER and ORR under different surface coverage of the oxygenated

species.

Acknowledgement

This study is based upon work supported by the National Science Foundation (NSF) under Grant No. 1945139, under the NSF 17-537 Faculty Early Career Development Program. We acknowledge computational support and resources from the computing facilities at University of North Texas (UNT) and the Center for Advanced Scientific Computing and Modeling (CASCaM). This research used computational resources of the Compute and Data Environment for Science (CADES) cluster at the Oak Ridge National Laboratory and of the National Energy Research Scientific Computing Center (NERSC), which were supported by the Office of Science of the U.S. Department of Energy under Contract Nos. DE- AC05-00OR22725 and AC02-05CH11231, respectively.

References

(1) Seh, Z. W.; Kibsgaard, J.; Dickens, C. F.; Chorkendorff, I.; Nørskov, J. K.; Jaramillo, T. F. Combining theory and experiment in electrocatalysis: Insights into materials design. *Science* **2017**, *355*.

(2) Man, I. C.; Su, H.-Y.; Calle-Vallejo, F.; Hansen, H. A.; Martínez, J. I.; Inoglu, N. G.; Kitchin, J.; Jaramillo, T. F.; Nørskov, J. K.; Rossmeisl, J. Universality in oxygen evolution electrocatalysis on oxide surfaces. *ChemCatChem* **2011**, *3*, 1159–1165.

(3) Viswanathan, V.; Hansen, H. A.; Rossmeisl, J.; Nørskov, J. K. Universality in oxygen reduction electrocatalysis on metal surfaces. *ACS Catal.* **2012**, *2*, 1654–1660.

(4) Greeley, J.; Stephens, I.; Bondarenko, A.; Johansson, T. P.; Hansen, H. A.; Jaramillo, T.; Rossmeisl, J.; Chorkendorff, I.; Nørskov, J. K. Alloys of platinum and

early transition metals as oxygen reduction electrocatalysts. *Nat. Chem.* **2009**, *1*, 552–556.

(5) Rossmeisl, J.; Logadottir, A.; Nørskov, J. K. Electrolysis of water on (oxidized) metal surfaces. *Chem. Phys.* **2005**, *319*, 178–184.

(6) Deng, D.; Novoselov, K.; Fu, Q.; Zheng, N.; Tian, Z.; Bao, X. Catalysis with two-dimensional materials and their heterostructures. *Nat. Nanotechnol.* **2016**, *11*, 218–230.

(7) Bonaccorso, F.; Colombo, L.; Yu, G.; Stoller, M.; Tozzini, V.; Ferrari, A. C.; Ruoff, R. S.; Pellegrini, V. Graphene, related two-dimensional crystals, and hybrid systems for energy conversion and storage. *Science* **2015**, *347*.

(8) Hinnemann, B.; Moses, P. G.; Bonde, J.; Jørgensen, K. P.; Nielsen, J. H.; Horch, S.; Chorkendorff, I.; Nørskov, J. K. Biomimetic hydrogen evolution: MoS2 nanoparticles as catalyst for hydrogen evolution. *J. Am. Chem. Soc.* **2005**, *127*, 5308–5309.

(9) Chia, X.; Pumera, M. Layered transition metal dichalcogenide electrochemistry: journey across the periodic table. *Chem. Soc. Rev.* **2018**, *47*, 5602–5613.

(10) Haastrup, S.; Strange, M.; Pandey, M.; Deilmann, T.; Schmidt, P. S.; Hinsche, N. F.; Gjerding, M. N.; Torelli, D.; Larsen, P. M.; Riis-Jensen, A. C., et al. The Computational 2D Materials Database: high-throughput modeling and discovery of atomically thin crystals. *2D Mater.* **2018**, *5*, 042002.

(11) Mounet, N.; Gibertini, M.; Schwaller, P.; Campi, D.; Merkys, A.; Marrazzo, A.; Sohier, T.; Castelli, I. E.; Cepellotti, A.; Pizzi, G., et al. Two-dimensional materials from high-throughput computational exfoliation of experimentally known compounds. *Nat. Nanotechnol.* **2018**, *13*, 246–252.

(12) Chia, X.; Eng, A. Y. S.; Ambrosi, A.; Tan, S. M.; Pumera, M. Electrochemistry of

nanostructured layered transition-metal dichalcogenides. *Chem. Rev.* **2015**, *115*, 11941–11966.

(13) Mak, K. F.; Lee, C.; Hone, J.; Shan, J.; Heinz, T. F. Atomically thin MoS 2: a new direct-gap semiconductor. *Phys. Rev. Lett.* **2010**, *105*, 136805.

(14) Voiry, D.; Mohite, A.; Chhowalla, M. Phase engineering of transition metal dichalcogenides. *Chem. Soc. Rev.* **2015**, *44*, 2702–2712.

(15) Wu, J.; Liu, M.; Chatterjee, K.; Hackenberg, K. P.; Shen, J.; Zou, X.; Yan, Y.; Gu, J.; Yang, Y.; Lou, J., et al. Exfoliated 2D transition metal disulfides for enhanced electrocatalysis of oxygen evolution reaction in acidic medium. *Adv. Mater. Interfaces* **2016**, *3*, 1500669.

(16) Li, P.; Zhu, J.; Handoko, A. D.; Zhang, R.; Wang, H.; Legut, D.; Wen, X.; Fu, Z.; Seh, Z. W.; Zhang, Q. High-throughput theoretical optimization of the hydrogen evolution reaction on MXenes by transition metal modification. *J. Mater. Chem. A* **2018**, *6*, 4271–4278.

(17) Yang, J.; Shin, H. S. Recent advances in layered transition metal dichalcogenides for hydrogen evolution reaction. *J. Mater. Chem. A* **2014**, *2*, 5979–5985.

(18) Li, H.; Tsai, C.; Koh, A. L.; Cai, L.; Contryman, A. W.; Fragapane, A. H.; Zhao, J.; Han, H. S.; Manoharan, H. C.; Abild-Pedersen, F., et al. Activating and optimizing MoS 2 basal planes for hydrogen evolution through the formation of strained sulphur vacancies. *Nat. Mater.* **2016**, *15*, 48–53.

(19) Jain, A.; Wang, Z.; Nørskov, J. K. Stable two-dimensional materials for oxygen reduction and oxygen evolution reactions. *ACS Energy Lett.* **2019**, *4*, 1410–1411.

(20) Karmodak, N.; Andreussi, O. Oxygen Evolution on MoS2 Edges: Activation through Surface Oxidation. *J. Phys. Chem. C* **2021**, *125*, 10397–10405.

(21) Jayabal, S.; Saranya, G.; Wu, J.; Liu, Y.; Geng, D.; Meng, X. Understanding the high-electrocatalytic performance of two-dimensional MoS 2 nanosheets and their composite materials. *J. Mater. Chem. A* **2017**, *5*, 24540–24563.

(22) Sadighi, Z.; Liu, J.; Zhao, L.; Ciucci, F.; Kim, J.-K. Metallic MoS 2 nanosheets: multifunctional electrocatalyst for the ORR, OER and Li–O 2 batteries. *Nanoscale* **2018**, *10*, 22549–22559.

(23) Karmodak, N.; Andreussi, O. Catalytic Activity and Stability of Two-Dimensional Materials for the Hydrogen Evolution Reaction. *ACS Energy Lett.* **2020**, *5*, 885–891.

(24) Andreussi, O.; Dabo, I.; Marzari, N. Revised self-consistent continuum solvation in electronic-structure calculations. *J. Chem. Phys.* **2012**, *136*, 064102.

(25) Fisicaro, G.; Genovese, L.; Andreussi, O.; Marzari, N.; Goedecker, S. A generalized Poisson and Poisson-Boltzmann solver for electrostatic environments. *J. Chem. Phys.* **2016**, *144*, 014103.

(26) Nattino, F.; Truscott, M.; Marzari, N.; Andreussi, O. Continuum models of the electrochemical diffuse layer in electronic-structure calculations. *J. Chem. Phys.* **2019**, *150*, 041722.

(27) Hörmann, N. G.; Andreussi, O.; Marzari, N. Grand canonical simulations of electrochemical interfaces in implicit solvation models. *J. Chem. Phys.* **2019**, *150*, 041730.

(28) Py, M.; Haering, R. Structural destabilization induced by lithium intercalation in MoS2 and related compounds. *Can. J. Phys.* **1983**, *61*, 76–84.

(29) Li, J.; Zhao, B.; Chen, P.; Wu, R.; Li, B.; Xia, Q.; Guo, G.; Luo, J.; Zang, K.; Zhang, Z., et al. Synthesis of Ultrathin Metallic MTe2 (M= V, Nb, Ta) Single-Crystalline Nanoplates. *Adv. Mater.* **2018**, *30*, 1801043.

(30) Dużyńska, A.; Judek, J.; Wilczyński, K.; Zberecki, K.; Łapińska, A.; Wróblewska, A.; Zdrojek, M. Temperature-induced phonon behavior in titanium disulfide (TiS2) nanosheets. *J. Raman Spectrosc* **2019**, *50*, 1114–1119.

(31) Nørskov, J. K.; Rossmeisl, J.; Logadottir, A.; Lindqvist, L.; Kitchin, J. R.; Bligaard, T.; Jonsson, H. Origin of the overpotential for oxygen reduction at a fuel-cell cathode. *J. Phys. Chem. B* **2004**, *108*, 17886–17892.

(32) Exner, K. S.; Over, H. Kinetics of electrocatalytic reactions from first-principles: a critical comparison with the ab initio thermodynamics approach. *Acc. Chem. Res.* **2017**, *50*, 1240–1247.

(33) Exner, K. S. Why approximating electrocatalytic activity by a single free-energy change is insufficient. *Electrochim. Acta* **2021**, *375*, 137975.

(34) Exner, K. S. Why the optimum thermodynamic free-energy landscape of the oxygen evolution reaction reveals an asymmetric shape. *Mater. Today Energy* **2021**, *21*, 100831.

(35) Huang, J.; Hörmann, N.; Oveisi, E.; Loiudice, A.; De Gregorio, G. L.; Andreussi, O.; Marzari, N.; Buonsanti, R. Potential-induced nanoclustering of metallic catalysts during electrochemical CO 2 reduction. *Nat. Commun.* **2018**, *9*, 1–9.

(36) Stan, R.-M.; Mahatha, S. K.; Bianchi, M.; Sanders, C. E.; Curcio, D.; Hofmann, P.; Miwa, J. A. Epitaxial single-layer NbS 2 on Au (111): Synthesis, structure, and electronic properties. *Phys. Rev. Mater.* **2019**, *3*, 044003.

(37) Wang, H.; Huang, X.; Lin, J.; Cui, J.; Chen, Y.; Zhu, C.; Liu, F.; Zeng, Q.; Zhou, J.; Yu, P., et al. High-quality monolayer superconductor NbSe 2 grown by chemical vapour deposition. *Nat. Commun.* **2017**, *8*, 1–8.

(38) Shi, J.; Wang, X.; Zhang, S.; Xiao, L.; Huan, Y.; Gong, Y.; Zhang, Z.; Li, Y.; Zhou, X.;

Hong, M., et al. Two-dimensional metallic tantalum disulfide as a hydrogen evolution catalyst. *Nat. Commun.* **2017**, *8*, 1–9.

(39) Dardel, B.; Grioni, M.; Malterre, D.; Weibel, P.; Baer, Y.; Levy, F. Spectroscopic observation of charge-density-wave-induced changes in the electronic structure of 2H-TaSe2. *J. Phys. Condens. Matter* **1993**, *5*, 6111.

(40) Shao, Y.; Song, S.; Wu, X.; Qi, J.; Lu, H.; Liu, C.; Zhu, S.; Liu, Z.; Wang, J.; Shi, D., et al. Epitaxial fabrication of two-dimensional NiSe2 on Ni (111) substrate. *App. Phys. Lett.* **2017**, *111*, 113107.

(41) Zhao, B.; Dang, W.; Liu, Y.; Li, B.; Li, J.; Luo, J.; Zhang, Z.; Wu, R.; Ma, H.; Sun, G., et al. Synthetic control of two-dimensional NiTe2 single crystals with highly uniform thickness distributions. *J. Am. Chem. Soc.* **2018**, *140*, 14217–14223.

(42) Ma, H.; Dang, W.; Yang, X.; Li, B.; Zhang, Z.; Chen, P.; Liu, Y.; Wan, Z.; Qian, Q.; Luo, J., et al. Chemical vapor deposition growth of single crystalline CoTe2 nanosheets with tunable thickness and electronic properties. *Chem. Mater.* **2018**, *30*, 8891–8896.

(43) Park, J. C.; Yun, S. J.; Kim, H.; Park, J.-H.; Chae, S. H.; An, S.-J.; Kim, J.-G.; Kim, S. M.; Kim, K. K.; Lee, Y. H. Phase-engineered synthesis of centimeter-scale 1T-and 2H-molybdenum ditelluride thin films. *ACS Nano* **2015**, *9*, 6548–6554.

(44) Gunasooriya, G. K. K.; Nørskov, J. K. Analysis of Acid-Stable and Active Oxides for the Oxygen Evolution Reaction. *ACS Energy Lett.* **2020**, *5*, 3778–3787.

(45) Li, H.; Kelly, S.; Guevarra, D.; Wang, Z.; Wang, Y.; Haber, J. A.; Anand, M.; Gunasooriya, G. K. K.; Abraham, C. S.; Vijay, S., et al. Analysis of the limitations in the oxygen reduction activity of transition metal oxide surfaces. *Nat. Catal.* **2021**, *4*, 463–468.

(46) Martincová, J.; Otyepka, M.; Lazar, P. Is single layer MoS2 stable in the air? *Chem. Eur. J.* **2017**, *23*, 13233–13239.

(47) Lv, D.; Wang, H.; Zhu, D.; Lin, J.; Yin, G.; Lin, F.; Zhang, Z.; Jin, C. Atomic process of oxidative etching in monolayer molybdenum disulfide. *Sci. Bull.* **2017**, *62*, 846–851.

(48) Tagawa, M.; Yokota, K.; Ohmae, N.; Matsumoto, K.; Suzuki, M. Hyperthermal Atomic Oxygen Interaction with MoS 2 Lubricants Relevance to Space Environmental Effects in Low Earth Orbit—Atomic Oxygen-Induced Oxidation. *Tribol. Lett.* **2004**, *17*, 859–865.

(49) Walter, T. N.; Kwok, F.; Simchi, H.; Aldosari, H. M.; Mohney, S. E. Oxidation and oxidative vapor-phase etching of few-layer MoS2. *J. Vac. Sci. Technol., B: Nanotechnol. Microelectron.: Mater., Process.* **2017**, *35*, 021203.

(50) Farigliano, L. M.; Paredes-Olivera, P. A.; Patrito, E. M. Initial Steps of Oxidative Etching of MoS2 Basal Plane Induced by O2. *J. Phys. Chem. C* **2020**, *124*, 13177–13186.